10/20/2008

Dear Dr. McIndoe,

Enclosed please find our progress report in the form of a submitted manuscript. A major purpose of the proposal was to test the hypothesis that early in the course of type 1 diabetes, apparent ion demand (as assessed by MEMRI) is abnormal within non-vascular retina. To this end we used the MMPC funds to examine intraretinal ion regulation using manganese-enhanced MRI (MEMRI) at various times after conversion of mice to diabetes using STZ to determine the time course of co-localized structural and functional patterns in inner and outer retina. In the manuscript these data are summarized in Figure 2 which illustrates, for the first time, distinct time periods during which intraretinal manganese uptake was first subnormal (1.5 – 4.2 mo of diabetes) followed by a relative increase (> 5.5 mo of diabetes). Importantly, these periods corresponded well with previously reported temporal windows when intervention with insulin therapy was either successful at inhibiting later histopathology (2 mo of diabetes) or not (6 mo of diabetes) (Exp Diabetes Res 2007;2007:21976). These considerations raise the strong possibility that while subnormal intraretinal uptake is an ominous development in emerging diabetic retinopathy, intervention during this time is most likely to be successful compared to starting treatment after the subsequent relative increase.

We have asked for and received a no-cost extension in light of our key assistants' maternity leave. Resumption of experiments will occur starting November 1st. With the limited funds remaining, we have decided to test the Ins2 Akita mouse, another mouse model that exhibits morphologic features similar to those found in patients with diabetic retinopathy and whose early retinal pathophysiology is poorly characterized. These studies will provide a necessary further test of our hypothesis that **early in the course of type 1 diabetes, apparent ion demand (as assessed by MEMRI) is abnormal within non-vascular retina** by comparing the temporal profile of intraretinal ion dysregulation in the Ins2 Akita to that in the STZ model. Our results in these two important, selected mice models will lay the groundwork in understanding that will allow for rapid testing of new mouse models of diabetic retinopathy as they become available and aid in the identification of promising pharmaceuticals, drug targets, and schedules for intervention based on MEMRI metrics. Such pre-clinical diagnosis and prognosis are not currently possible.

Bruce Berkowitz

[For Investigative Ophthalmology and Visual Science]

Retinal Ion Regulation in a Mouse Model of Diabetic Retinopathy: Natural History and the Effect of Cu/Zn Superoxide Dismutase Overexpression

Bruce A. Berkowitz[1, 2], Marius Gradianu[1], David Bissig[1],
Timothy S. Kern[3], and Robin Roberts[1]

[1]Dept. of Anatomy and Cell Biology, Wayne State University, Detroit, MI; [2]Dept. Of Ophthalmology, Wayne State University, Detroit, MI; [3]Dept. of Medicine, Case Western Reserve University

Correspondence: Bruce A. Berkowitz, Ph.D.
Department of Anatomy and Cell Biology
Wayne State University School of Medicine
540 E. Canfield
Detroit, MI 48201
(313) 577-9035
(313) 577-3125 (FAX)
baberko@med.wayne.edu (e-mail)

Word count: 4,747

Purpose: To test the hypotheses that manganese-enhanced MRI (MEMRI) is useful in evaluating intraretinal ion dysregulation in wildtype and Cu/Zn superoxide dismutase (SOD1) overexpressor mice.
Methods: Central intraretinal ion activity and retinal thickness were measured from high resolution data of these groups: light and dark adapted wildtype C57BL/6 (WT) mice (to gauge MEMRI sensitivity to normal visual processing in mice), and dark-adapted diabetic and non-diabetic WT and Cu/Zn superoxide dismutase overexpressor (SOD1OE) mice. Glycated hemoglobin and retinal vascular histopathology were also determined.
Results: In WT mice, light adaptation reduced outer retinal manganese uptake compared with that in dark adaptation; no effect on inner retinal uptake was found. In diabetic WT mice, intraretinal manganese uptake became subnormal between 1.5 and 4 mo of diabetes and then relatively increased. Central retinal thicknesses, as determined with MEMRI, decreased as a function of age in diabetic mice but remained constant in control mice. Non-diabetic SOD1OE mice had normal retinal manganese uptake but subnormal retinal thickness and supernormal acellular capillary density. At 4.2 mo of diabetes, SOD1OE mice had normal manganese uptake and no further thinning; acellular capillaries frequency did not increase by 9-10 mo of diabetes.
Conclusions: In emerging diabetic retinopathy, MEMRI provided an analytic measure of an ionic dysregulatory pattern that was sensitive to SOD1 overexpression. The potential benefit of SOD1 overexpression to inhibit retinal pathology in this model is limited by the retinal and vascular degeneration that develops independently of diabetes.

Microvascular pathology is the clinical hallmark of diabetic retinopathy. Yet, functional losses occur in the retina between the onset of hyperglycemia and the appearance of ophthalmoscopically visible microangiopathy. In this period of emergent diabetic retinopathy, dysfunction occurs not only in vascular retina (e.g., autoregulatory impairment), but also in non-vascular retina (e.g., reduced contrast sensitivity, relatively lower retinal electrophysiologic parameters, and subnormal ion regulation) (1-16). The importance of such functional impairments is underscored by noting that correction of early diabetes-induced retinal dysfunctionality, such as abnormal ion regulation, is linked with the inhibition of late-stage vascular histopathology (17-19). For example, in experimental diabetes, preventative pharmaceutical treatment with captopril can inhibit early reductions in a major regulator of ion homeostasis in the retina, Na/K ATPase activity, and ameliorate late stage vascular histopathology development (19;20). These associations are suggestive and more work is needed to better define the factors regulating diabetes-induced subnormal retinal ion activity.

Pathobiochemistry, such as oxidative stress, are also strongly linked with developing diabetic retinopathy. However, few studies have investigated the interplay between early diabetes-induced ion dysregulation and oxidative stress. Treating diabetic rats with α-lipoic acid corrected diabetes-induced reductions in retinal antioxidants such as manganese superoxide dismutase (SOD2) and Cu/Zn superoxide dismutase (SOD1)(21;22). The same treatment inhibited early ion dysregulation, as well as late-stage vascular histopathology such as degeneration of retinal capillaries (17). Recent elegant work involving SOD2 overexpressor mice has established an important role of SOD2 in diabetic retinopathy (21;23;24). SOD1 constitutes at least 85% of the total cellular superoxide dismutase activity in many mammalian cells, has high activity in the retina, and is a key defense against superoxide-related oxidative stress in the cytosol and intermembrane space of mitochondria (25-27). Efforts to understand the role of SOD1 in non-diabetic models of retinal injury using SOD1 overexpressor mice have produced mixed result, with overexpression either increasing retinal neuronal damage, providing neuroprotection, or having no effect (28-30). Despite strong evidence that diabetes causes an early oxidative stress environment in retinas from rats and mice (24;31-33), and anti-

oxidant therapy inhibits the later degeneration of the retinal capillaries, a specific role of SOD1 in diabetic retina has not been well studied.

One powerful non-invasive method for studying cellular ionic activity is manganese-enhanced MRI (MEMRI) (34;35). MEMRI allows for non-invasive measurement of retinal thickness, and, notably, layer-specific uptake of manganese (Mn^{2+}) ion following systemic $MnCl_2$ injection (17;36-38). Manganese ion, an MRI contrast agent and analog of, for example, calcium, readily accumulates intracellularly as a function of membrane integrity and cellular activity, is sensitive to Na/K ATPase activity, and is relatively slowly removed (34;36;39-41). In rat models of diabetic retinopathy and in a non-diabetic rat ischemia / reperfusion model which produces similar histopathology to diabetic retinopathy, impaired ion regulation developed prior to the appearance of neuronal and vascular degeneration (17;36-38). Such changes in retinal ion regulation in mouse models of diabetic retinopathy have not yet been reported.

In this study, we evaluated the sensitivity of MEMRI to normal changes in retinal ion regulation with light and dark adaption (i.e., visual processing) in the mouse retina *in vivo*. Next, we describe the nature history of MEMRI changes before and during the appearance of acellular capillaries in mice. In addition, we compared the effect of diabetes in wildtype (WT) mice and transgenic mice which overexpress SOD1 on intraretinal ion regulation and thickness, and vascular histopathology. If increased oxidative stress were playing an important role in altering ion homeostasis in diabetic retinopathy, then upregulation of SOD1 activity would be expected to be protective against early ion dysregulation and, possibly, late stage histopathology (30).

Research Design and Methods

The animals were treated in accordance with the 'Principles of laboratory animal care' (NIH publication no. 85–23, revised 1985; http://grants1.nih.gov/grants/olaw/references/phspol.htm), as well as the Association for Research in Vision and Ophthalmology (ARVO) Statement on Animals in Vision research.

Groups: For visual processing comparisons, different groups of female C57BL/6 mice (WT, n = 4 per condition, average age = 3 months, Hilltop Lab Animals, Inc., PA) were studied using a light and dark adaptation procedure previously described in rats

(40). Natural history studies were conducted with the following male C57BL/6 groups that were diabetic (chronologic age / diabetes-duration): 3.6 mo / 0.9 mo, n = 5; 4.1 mo / 1.5 mo, n = 5; 5.2 mo / 2.5 mo, n = 6; 8.2 mo / 5.5 mo, n = 6; 10 mo / 7.4 mo, n = 4 (The Jackson Laboratory, ME). An additional group, from Hilltop Animals, Inc., PA, was also studied: 7.2 mo / 4 mo, n = 5. The following non-diabetic control mice were examined: chronologic age: 3.3 mo, n =7; 4.9 mo, n = 5; 8 mo, n = 3 (The Jackson Laboratory, ME), or 7.4 mo, n = 6 (Hilltop Lab Animals, Inc., PA). The effect of SOD1 overexpression was examined in the following two groups of C57BL/6 mice: SOD1OE control (SOD1OE, n = 4 males, average age 5 mo, The Jackson Laboratory, ME) and diabetic male SOD1 overexpressor mice (SOD1OE+D, n = 4 males, 4.2 mo diabetic, age 7.1 mo, The Jackson Laboratory, ME). SOD1OE mice have a 2-3 fold increase in central nervous system SOD1 activity (42;43)(http://jaxmice.jax.org/strain/002629rf.html). Importantly, it has been reported that diabetes had no effect on the extent of SOD1 overexpression (42).

Diabetes was induced in mice with a starting weight of 20–24 g by streptozotocin (60 mg/kg; 10 mM citrate buffer [pH 4.5]) intraperitoneal injection once a day for 5 consecutive days. Body weight and blood glucose levels were monitored weekly. Insulin (neutral protamine Hagedorn [NPH]) was administered to allow slow weight gain while maintaining hyperglycemia (blood glucose levels above 400 mg/dL). Normal rodent chow and water were provided ad libitum. All mice were housed in normal 12 hour cycled lab lighting until the end of the experiment. Glycated hemoglobin was measured from blood collected after each MEMRI experiment (Glyco-Tek affinity columns, kit 5351; Helena Laboratories, Beaumont, TX). After 4 months of diabetes, only those mice with blood glucose levels higher than 400 mg/dL were studied via MEMRI.

High resolution MRI: All mice were maintained in darkness for 16 - 20 hours prior to manganese injection. Procedures (e.g., weighing, injecting $MnCl_2$, anesthetic administration, and MRI exam) were done under dim red light or darkness. $MnCl_2$ was administered as an intraperitoneal injection (66 mg/Kg) on the right side of awake mice. Following this injection, mice were maintained in dark conditions for another 3.5 - 4 hours. Immediately before the MRI experiment, mice were anesthetized using urethane (36% solution, i.p., 0.083 ml / 20 g animal weight, prepared fresh daily, Aldrich, Milwaukee, WI) and xylazine (1-8 mg/kg, ip). We found that urethane alone tended to

increase respiratory frequency of the mice and thus motion artifacts on MEMRI. The addition of a small amount of the muscle relaxant xylazine minimized these artifacts. Core temperatures were maintained using a recirculating heated water blanket. MRI data were acquired on a 4.7 T Bruker Avance system using a two-turn transmit/receive surface coil (1.0 cm diameter) placed over the eyes. A single transverse slice through the center of the eye (based on sagittal localizer images collected using the same adiabatic pulse sequence as above) was obtained for each mouse. Transverse images were then acquired using an adiabatic spin-echo imaging sequence (repetition time TR 350 s, echo time TE 16.7 ms, number of acquisitions NA 16, sweep width 61728 Hz, matrix size, 512 x 512, slice thickness 620 μm, pixel size 23.4 x 23.4 x 620 μm^3, field of view 12 x 12 mm^2) (44). After the MEMRI exam, a final blood sample was obtained for glycated hemoglobin analysis and mice were humanely euthanized.

Histopathology: A separate batch of non-diabetic and diabetic SOD1OE mice, made diabetic at the same time as those studied by MEMRI, were sent to Dr. Kern's lab and aged until 9-10 mo before histopathologic examination. Age-matched wild-type control mice were maintained during this same time period in Dr. Kern's lab and were used for comparison. The retinal vasculature was isolated by the trypsin digest method as described by us previously (45;46). Briefly, freshly isolated eyes were fixed with buffered formalin (4% [wt/vol.] formaldehyde, 0.075 mol/l sodium phosphate buffer). Retinas were isolated, washed in water overnight and then incubated with 3% Difco crude typsin (BD, Sparks, MD, USA) at 37°C for 1 h. Non-vascular cells were gently brushed away from the vasculature, the isolated vasculature was mounted on glass slides, air-dried and stained with periodic acid–Schiff and haematoxylin (PASH).

Data Analysis:

Layer specific signal intensity: For visualization purposes, in-house written software was used to map the *in situ* image into a linear representation for each retina. Within each group, linearized retinas were averaged into a composite image. For quantitative analysis, signal intensities were first extracted from each mouse image using the program NIH IMAGE and derived macros (47) and the results from that group compared with a generalized estimating equation approach (described below) (40). Changes in receiver gain between animals were controlled for by setting the signal

intensity of a fixed region of noise in each mouse to a fixed value. Other tissues within the sensitive volume of the coil may also be affected by diabetes with differential enhancement following manganese injection and so were considered inadequate as internal references. Post-receptor (or inner retina) and receptor (or outer retina) signal intensity data (from the edge of the optic nerve to 1 mm from the center of the optic nerve) were extracted as follows. As we have previously discussed, the inner / outer retinal division is observable in light adapted retina (based on contrast generated by the differential amount of manganese taken up in inner and outer retina) but is not observable in dark adapted retinas (see Figure 1)(40). Thus, we take advantage of the fact that whole retina thickness values are within normal range for mice and assume that the division between inner and outer retina and between retina and choroid occur as in normal retina (about 100 μm from the vitreal-retinal border (or about 4 pixels (23.4 x 4 = 96 μm) for inner retina, and then 3 pixels posterior to this region to sample the outer retina. To further ensure that we are measuring from inner and outer retina, the pixel values just anterior each of these divisions were designated as representative of inner or outer retinal values, respectively. These regions are illustrated in Figure 1. Data were analyzed as previously described (40).

Note that in Hilltop animals, no difference ($P > 0.05$) in extent of manganese uptake in inner retina after dark adaptation was found between male (80.5 $\pm$ 1.2 a.u., n = 6, mean $\pm$ SEM) and female (84.1 $\pm$ 1.1 a.u., n = 4) mice, and these data were combined for further comparisons.

Extraocular muscle signal intensity: To assess a possible role for differences in systemic handling of manganese, for each mouse, the mean signal intensity was measured from a fixed-size ellipse-shaped region-of-interest drawn in the anterior-most aspect of the inferior rectus muscle. Mice that did not have a recognizable rectus muscle due to head and slice orientation were not included in the extraocular muscle analysis. Extraocular muscle signal intensities from diabetic and control Hilltop mice were, respectively, 14 – 27% lower ($P < 0.05$) than that from Jackson lab mice (data not shown) suggesting that differences in inner retinal uptake might be secondary to differences in systemic handling of manganese. Similarly aged control dark adapted mice had inner retinal uptake of manganese in mice from Hilltop mice (81.9 $\pm$ 0.8 a.u., n = 10) that were lower ($P < 0.05$)

than that in mice from Jackson mice (90.8 $\pm$ 0.8 a.u., n = 12). Thus, intraretinal data of mice from Hilltop mice were scaled by multiplying by 1.11 to allow for comparisons with data of Jackson mice. The reason for the vendor-difference is not clear but may represent a combination of differences in the genetics of the founder mice, and genetic drift within each colony. In addition, we note that in a previous study in non-diabetic rats, simply reducing the injected dose of $MnCl_2$ by a factor of 2.9 (from 44 to 15 mg/kg) did not result in a decrease ($P > 0.05$) in intraretinal signal intensity 4 hours after injection (data not shown). Thus, the present vendor differences may reflect variations in organ or metabolic handling of manganese and not simple differences in plasma manganese levels. In any event, a straightforward tissue-specific scalar normalization was adequate for removing these vendor specific variations.

Retinal Thickness: Whole retinal thicknesses were determined from each MEMRI-generated image as the radial distance between the anterior edge and the posterior edge of the retina at distances $\pm$ 0.4 – 1 mm from the optic nerve, as previously described (48). Briefly, in-house written software was used to map the *in situ* image into a linear representation for each retina. Thicknesses were derived from these linearized images. First, the average signal intensity profile as a function of depth into the retina was determined by the program. Then the point at which the signal intensity profile crosses the average of the highest and lowest signal intensity near provisional vitreous/retina and retina/choroid+sclera boundaries was calculated automatically. The distance between these two mid-points was considered the whole retinal thickness. No difference was noted when automatically derived whole retinal thicknesses were compared with manually derived thickness (data not shown). Mean superior and inferior retinal values generated for each animal group were combined and used for comparisons.

Histopathology: Acellular capillaries were quantitated in 6-8 field areas in the mid-retina (400X magnification) in a masked manner. Acellular capillaries were identified as capillary-sized vessel tubes having no nuclei anywhere along their length, and were reported per square millimeter of retinal area. Tubes have a diameter <30% of the diameter of adjacent capillaries were identified as strands, and not counted as acellular capillaries. Acellular capillaries for animals from all 4 groups were measured by the same reader (TSK) at the same time and in a masked manner.

Statistical Analysis: Comparisons of MEMRI retinal signal intensities were performed using a generalized estimating equation (GEE) approach (40;49). GEE performs a general linear regression analysis using all of the pixels in each subject and accounts for the within subject correlation between adjacent pixels. The retinal thickness data were consistent with a normal distribution and comparisons between groups were performed using an unpaired 2-tailed t-test analysis. Histology data were analyzed by the nonparametric Kruskal–Wallis test followed by the Mann–Whitney *U* test. In all cases, two-tailed $P < 0.05$ was considered statistically significant, unless otherwise noted. Data are presented as mean $\pm$ SEM.

Results

Systemic physiology: Over the study duration, WT control mice had constant body weights (range 28.1 – 30.3 g) or glycated hemoglobins (5.2 – 5.8 %). Further comparisons were performed using the average WT body weight of 30.5 $\pm$ 0.6 g and glycated hemoglobin of 5.7 $\pm$ 0.1 % (n = 21, mean $\pm$ SEM). Within the WT diabetic group, body weights (24.6 – 26.4 g) and glycated hemoglobins (10.6 – 13.9 %) did not differ from each other ($P > 0.05$), but both parameters were different ($P < 0.05$) than the above average WT values. The body weights of the SOD1OE (27.4 $\pm$ 1.5 g) and SOD1OE+D (24.8 $\pm$ 1.0 g) groups were different ($P < 0.05$) from controls. Glycated hemoglobin values for SOD1OE mice (5.1 $\pm$ 0.2 %) were not different from controls ($P > 0.05$) while that of the SOD1OE+D group (10.9 $\pm$ 0.7 %) were.

MEMRI:

Effect of light adaptation: In WT mice, light and dark adapted retinas had similar ($P > 0.05$) inner retinal signal intensities, but different ($P < 0.05$) outer retinal intensities (Figure 1).

Effect of diabetes:

Natural history:

Controls: In non-diabetic WT mice between 3.5 and 8 mo of age, no significant differences ($P > 0.05$) were noted in signal intensity of either inner (87.6 – 95.3 a.u.) or outer (86.1 – 93.1 a.u.) retina. Thus, average WT signal intensity for inner (n = 21, 91.1 $\pm$

0.6 a.u.) and outer (89.2 ± 0.6 a.u.) retina were used for comparison with the diabetic data of similarly aged mice.

Diabetic: At 0.9 and 5.5 mo of diabetes (3.5 and 8.2 mo chronological age), the degree of manganese uptake in inner and outer retina was not different from the above average WT values over this age range ($P > 0.05$); no age-matched controls were available for comparisons to the 7.4 mo diabetic (10 mo chorological age) data (Figure 2). The extent of inner and outer retinal uptake was similarly subnormal ($P < 0.05$) between 1.5 and 4.2 mo of diabetes. Compared to the combined 1.5 - 4.2 diabetic data, intraretinal signal intensities at 0.9, 5.5, and 7.4 mo of diabetes were relatively increased ($P < 0.05$).

To investigate the possibility that systemic alterations affected the above retinal pattern, signal intensities of non-neuronal extraocular muscle of diabetic WT mice and age-matched controls were compared. As expected, extraocular muscle signal intensity increased after manganese injection (data not shown). Extraocular muscle intensity of 1.5 – 4.2 mo diabetic mice (73.9 ± 2.0 a.u., n = 16) were not different ($P > 0.05$) from that of age-matched WT mice (73.1 ± 3.0 a.u., n = 12).

Effect of SOD1 overexpression: Compared with the above average WT values, non-diabetic and diabetic SOD1OE mice had normal inner and outer retinal signal intensities ($P > 0.05$) (Figure 3).

Retinal thickness: In control mice, whole retinal thickness (range 195 – 230 μm) remained constant with aging ($r = 0.07$, $P = 0.75$) and the data were combined to produce a mean WT thickness of 211 ± 2 μm (n = 21). In diabetic mice a similar range of thickness was noted (183 – 234 μm) and the mean thickness (209 ± 2 mm) was not different ($P > 0.05$) from controls values. As diabetic mice aged, retinal thickness decreased in a linear fashion (thickness = 216 – 2*(duration of diabetes), $r = - 0.4$, $P = 0.02$). Non-diabetic 5 mo old SOD1OE mice had an average retinal thickness (197 ± 2 μm) that was different ($P < 0.05$) than that of age-matched control WT mice and 4.2 mo diabetic SOD1OE mice (211 ± 3 μm).

Histopathology: In WT mice, 9-10 months of diabetes caused a significant increase ($P < 0.05$)-in the number of degenerate retinal capillaries (Figure 4). Non-diabetic SOD1OE mice had more degenerate capillaries than did wildtype non-diabetic

mice ($P < 0.05$). Compared to age-matched non-diabetic SOD1OE mice, diabetes did not cause any further increase in capillary degeneration in SOD1OE mice ($P > 0.05$) (Figure 4).

Discussion

In this study, the following three major results were found. 1) In WT mice, layer-specific MEMRI data correlated with normal physiology associated with light and dark visual processing. These results support and extend our previous work which demonstrated similar intraretinal light / dark changes in the rat (40). 2) In diabetic WT mice, we found a diabetes-duration dependant evolution in uptake of manganese in photoreceptor and post-receptor retina. These associative observations, discussed in more detail below, are consistent with and broaden our prior report in with diabetic rats that reduced retinal manganese uptake occurred early in the time course and reflected a decrease in ion regulation within the retina (17). 3) Diabetic SOD1OE mice, unlike diabetic WT mice, had normal intraretinal manganese uptake. Non-diabetic SOD1OE mice had modest but significant retinal thinning and vascular degeneration, raising questions about the suitability of overexpression SOD1 as a means of inhibiting diabetic retinopathy. Nonetheless, the present results support the use of MEMRI in murine models as a powerful, objective, and non-invasive approach to measure early intraretinal ion dysregulation by, for example, oxidative stress.

The dose of $MnCl_2$ used in the present study (66 mg/kg) is not expected to adversely affect retinal function or anatomy. Previously, we established that a 33% lower dose of $MnCl_2$ (44 mg/kg) was not associated with changes in retinal function as assessed with ERG parameters at either 4 hrs or 7 days post injection, relative to control rats (36). In addition, at 30 days post-injection, whole and inner retinal thickness, intraocular pressure, and blood retinal barrier permeability surface area product were not different from that of control rats (40). However, in a preliminary study, the 44 mg/kg dose of $MnCl_2$ did not produce reliable contrast changes in the mouse retina, possibly due to the relatively higher overall metabolic rate in the mouse (data not shown). Instead, it was found empirically that a somewhat higher dose of manganese (66 mg/kg) produced more robust retinal contrast changes. This dose is similar to, or lower than, that used in other

mouse MEMRI studies, and is well below that needed to induce neurotoxicity (35;50). Thus, it is reasonable to consider the 66 mg/kg dose as non-toxic and the intraretinal uptake of manganese as a quantitative biomarker of ion activity regulation *in vivo*.

In previous rat studies, MEMRI was validated in rats as providing an accurate measure of retinal thickness without choroidal contamination (36;40). In this study the mean MEMRI-measured retinal thickness from WT mice (195 – 230 μm) was similar to the range in the literature for mice (187 – 225 μm) (51-53). In addition, the MEMRI data were consistent with the expected whole retinal thinning that coincides with increasing duration of diabetes, as reported in another mouse study (6;17;51). Retinal thickness data from SOD1OE mice are discussed below. These considerations support the use of MEMRI as a spatially accurate approach for evaluating whole retinal thickness in rodents.

We have previously demonstrated that, in the rat, intraretinal manganese uptake patterns robustly correlated with normal retinal physiology responses associated with light and dark visual processing (40). Normally, in dark adapted retina, ion activity and demand in photoreceptors increases via opening of cGMP-gated ion channels to generate the "dark current". In light adapted retina, photoreceptors hyperpolarize in response to light via closure of the cGMP-gated ion channels by way of the phototransduction cascade. Thus, the activity and ion demand of photoreceptors are increased in the dark and attenuated in the light. The situation in the inner retina is more complex. When the retina is dark adapted, the OFF pathway (OFF bipolar cell to OFF ganglion cell) is active in the inner retina; conversely, in the light, the ON pathway (ON bipolar cell to ON ganglion cell) is depolarizing. With equal representation of ON and OFF cells (bipolar and ganglion cells) in the retina, changes in inner retina activity caused by light or dark adaptation would be expected to be relatively equal. The light / dark results herein (Figure 1) provide additional support for the use of MEMRI as a sensitive probe of normal retinal physiology.

In this study, as in a previous report, control animals demonstrated relatively consistent intraretinal signal intensities over the months of this study (54). These data provide confidence in the reliability of the MEMRI exam. After 0.9 mo of diabetes, no significant change in intraretinal ion regulation from control values was noted. These

results are consistent with a lack of retinal toxicity of streptozotocin (4). Between 1.5 and 4.2 mo of diabetes, a significant and sustained decrease in retinal uptake of manganese occurs which was reminiscent of previous reports of subnormal uptake measured between 3 and 4.5 mo of diabetes in diabetic rat models (17). The mechanism involved with reduced retinal manganese uptake is not yet understood. One possible explanation is that the observed retinal ion dysregulation is secondary to diabetes-induced systemic changes in, for example, baseline plasma or tissue manganese levels. Clinically, baseline plasma levels of manganese are not different between patients with and without diabetes (55;56). Experimentally, large decreases in plasma manganese concentrations with diabetes are not expected since, in diabetic rats manganese levels in retina, and other tissues, are not different from that in controls (17;57). To further address this issue, we assumed that manganese uptake in muscle mirrored how each animal systemically handled manganese following intraperitoneal injection since muscle does not have a blood barrier. No differences in extraocular muscle manganese uptake were noted. When all of the above results are considered, we find no compelling evidence that systemic effects of diabetes contributes to the present observations.

Since impaired retinal ion regulation between 0.9 and 4.2 mo of diabetes preceded the onset of retinal cellular loss, it is unlikely to be a consequence of degeneration. A likely alternative explanation for the subnormal uptake results herein involves hyperglycemic increases in lipid peroxidation and protein glycation which could reduce the activity of major membrane-bound regulators of ion homeostasis (e.g., Na^+/K^+-ATPase, calcium ATPase, and ion exchangers) in retina (12;33). Previously, we reported in controls rats, that inhibition of retinal Na^+/K^+-ATPase activity using ouabain resulted in subnormal intraretinal manganese uptake (36).

At 5.5 and 7.4 mo of diabetes, the extent of retinal manganese uptake significantly increased relative to that at 1.5 – 4.2 mo of diabetes to normal levels. This relative increase is consistent with a previously indentified pattern in two different non-diabetic models in which a similar relative elevation in intraretinal manganese uptake from subnormal levels occurred with vascular and/or neuronal degeneration (58). We speculate that this subsequent increase in intraretinal manganese uptake is indicative of a gradual and abnormal opening of ion channels which eventually leads to calcium overload,

apoptosis, and vascular and neuronal cellular loss (59). Importantly, in diabetic retinopathy and in retinopathies with similarities to diabetic retinopathy, therapies which prevent this relative increase are strongly linked with neuro- and vasculo-protection (17;36). In particular, it is noteworthy that in diabetic rodents, late development of vascular histopathology continues even if good glycemic control is reinitiated at 6 mo of hyperglycemia, after the relative increase in intraretinal manganese uptake, but not if good control is started at 2 mo diabetes when manganese uptake is subnormal (60). These considerations highlight the extent of intraretinal manganese uptake as a robust biomarker in emerging diabetic retinopathy.

In this study, intraretinal ion regulation of diabetic SOD1OE mice was evaluated only at a single point raising the potential concern that subnormal uptake might have developed earlier or later than the measurement time point. We do not consider either possibility likely in light of strong link between the early intraretinal ionic dysregulatory pattern described above and later retinal degeneration, and lack of evidence for diabetes-induced degeneration in the diabetic SOD1OE retina. Retinas from C57BL/6 mice can develop more capillary degeneration than that measured here in the diabetic SOD1OE mice (61). Thus, it seems reasonable to postulate that diabetes had the potential to cause more vascular degeneration than was found in the present study. In addition, the diabetic SOD1OE uptake data are consistent with previous findings that α-lipoic acid treatment prevented early intraretinal ion dysregulation and later development of histopathology (17).

In non-diabetic SOD1OE mice, we found decreased body weight, and modest neuronal (retinal thinning) and vascular (acellular capillaries) degeneration but normal intraretinal uptake of manganese. This pattern is consistent with the ionic dysregulatory pattern linked with degeneration discussed above. Non-diabetic SOD2 overexpressor mice do not display these morphometric abnormalities (23). The reason for this histological difference with the present SOD1OE data is not clear. One possible explanation for the presence of retinal neuronal and vascular degeneration might involve SOD1 overexpression resulting in increased production of hydrogen peroxide in the cytosol (62;63) relative to the level of activity of its detoxification enzyme catalase. Several studies have hypothesized that non-diabetic SOD1OE mice would demonstrate

reduced retinal neuronal and / or vascular anatomical damage following various types of injury (28-30). Yet support for this hypothesis has been ambiguous (28-30). Notably, Levkovitch-Verbin et al. found that SOD1OE mice had exacerbated retinal ganglion cell death following optic nerve injury (28).

In conclusion, MEMRI was shown to be sensitive to physiologic changes in intraretinal ion regulation in mice. Our data in diabetic rodents support a key role of increased oxidative stress in general, and superoxide ion in particular, in the diabetes-induced reduction in intraretinal manganese uptake (17). Intriguingly, we identified distinct time periods during which intraretinal manganese uptake was first subnormal (1.5 – 4.2 mo of diabetes) followed by a relative increase (> 5.5 mo of diabetes). These periods corresponded well with previously reported temporal windows when intervention with insulin therapy was either successful at inhibiting later histopathology (2 mo of diabetes) or not (6 mo of diabetes) (60). These considerations, and those from other studies (64), raise that possibility that while subnormal intraretinal uptake is an ominous development in emerging diabetic retinopathy, intervention during this time is most likely to be successful compared to starting treatment after the subsequent relative increase.

Acknowledgements

Supported by NIH EY010221 (BAB), EY00300 (TSK), Juvenile Diabetes Research Foundation (BAB), the National Mouse Metabolic Phenotyping Centers Pilot & Feasibility Program (BAB), and an unrestricted grant from Research to Prevent Blindness (Kresge Eye Institute).

Figure Legends

Figure 1: MEMRI changes in murine inner and outer retinal signal intensity with light and dark adaptation. A) Representative MEMRI of a WT mouse eye. White arrows indicate the region illustrated in B). B) Pseudocolor linearized images of average retinal signal intensity in central retina of WT mice (left, light adapted, n = 4, and right, dark adapted, n =4). The same pseudocolor scale was used for both linearized images, where *blue* to *green* to *yellow* to *red* represent lowest to highest signal intensity. *Dotted black line*: boundary between inner and outer retina as demonstrated in previous studies (40). The intraretinal locations from which inner retinal (IR) and outer retinal (OR) data were extracted and used in this study are indicated by the black arrows on the right of the dark adapted linearized image. C) Summary of inner and outer retinal signal intensities in light and dark adapted mice. The numbers of animals used to generate these data are listed above each bar. Error bars represent the standard error of the mean. Comparisons were performed between inner retinal signal intensities during light or dark adaptation and between outer retina values during the different adaptation conditions. *, $P < 0.05$ was considered significant. The y-axis scale starts at 50 because this is the pre-manganese baseline level determined from uninjected mice (data not shown).

Figure 2: Summary of natural history of signal intensities for A) inner retina and B) outer retina. Grey symbols represent average WT inner or outer retinal intensities. *, $P < 0.05$, 2-tailed, compared with average WT inner (91.0 $\pm$ 0.6 a.u., n = 21) or outer (89.1 $\pm$ 0.6 a.u.) retinal intensities. %, $P < 0.05$, 2-tailed, compared with average inner (75.8 $\pm$ 0.6 a.u., n = 21) or outer (76.6 $\pm$ 0.6 a.u.) from mice with 1.5 - 4.2 mo of diabetes. Error bars are SEM. The y-axis scale starts at 50 because this is the pre-manganese baseline level determined from uninjected mice (data not shown).

Figure 3: Summary of changes in MEMRI intraretinal signal intensity in control and diabetic WT and SOD1OE mice. The y-axis scale starts at 50 because this is the pre-manganese baseline level determined from uninjected mice (data not shown). Significant comparisons to control inner or outer retina intensities are shown with a * for $P < 0.05$. Error bars are SEM and numbers over bars are numbers of animals studied.

Figure 4: Plot of number of degenerate retinal capillaries (acellular capillaries) in diabetic WT mice (9 mos of study, WT+D) compared to that in non-diabetic controls (WT) (left panel), and diabetic SOD1OE mice (SOD1+D) relative to that in non-diabetic SOD1OE controls (SOD1) (right panel). Diabetes-induced capillary degeneration was increased in WT (WT+D) but not SOD1 overexpressor (SOD1+D) mice. The numbers of animals used to generate these data are listed above each bar. Error bars represent the standard error of the mean. *, $P < 0.05$ was considered significant.

Figure 1

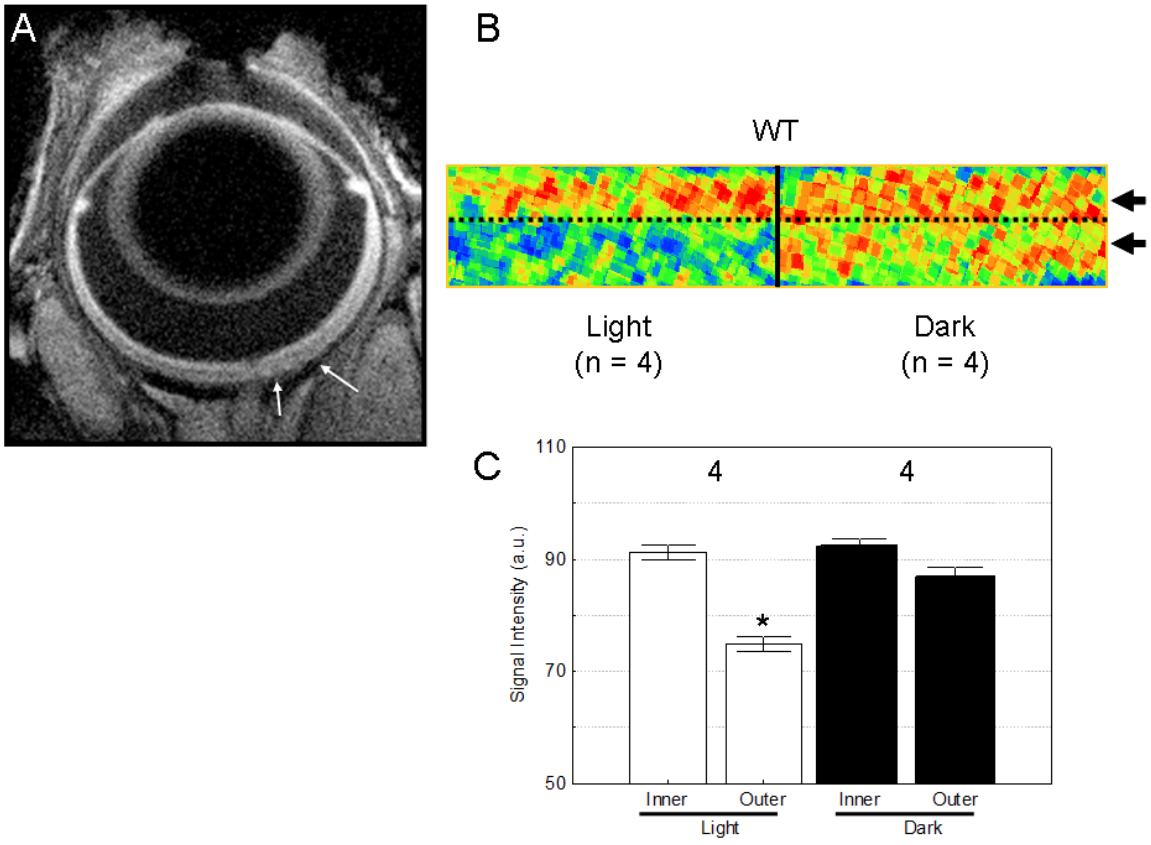
A
B
WT
Light
(n = 4)
Dark
(n = 4)
C
110
90
70
50
Signal Intensity (a.u.)
4
4
*
Inner
Outer
Inner
Outer
Light
Dark

Figure 2

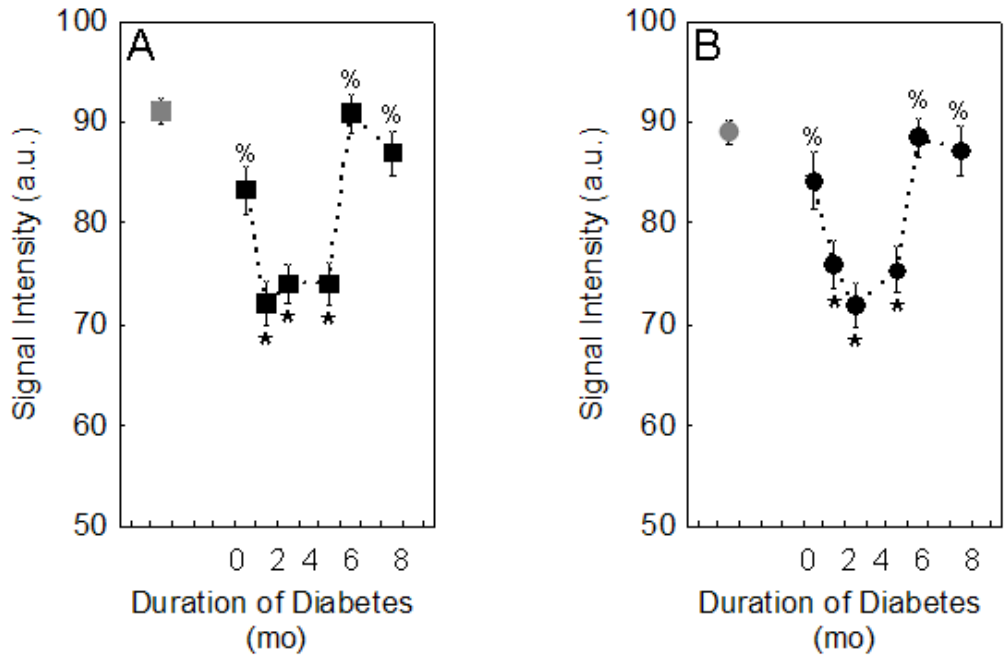
A
B
100
90
80
70
60
50
Signal Intensity (a.u.)
0 2 4 6 8
Duration of Diabetes
(mo)
%
*

Figure 3

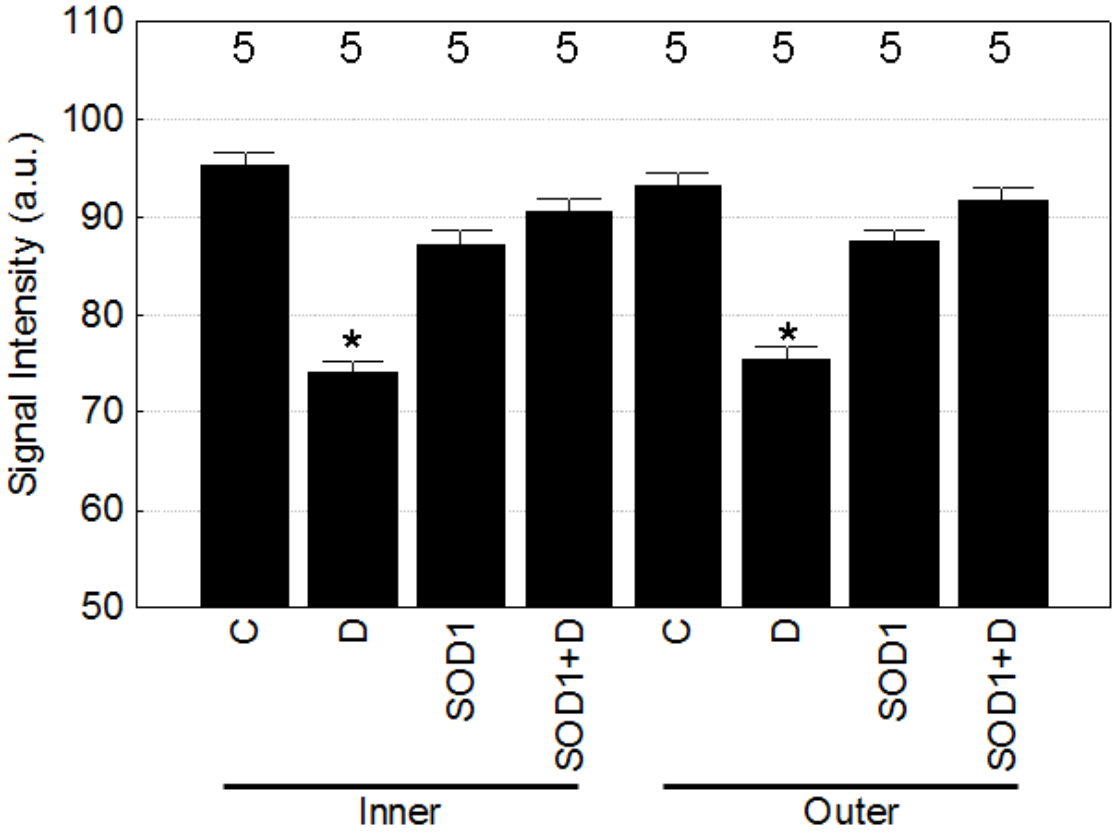
110
100
90
80
70
60
50
Signal Intensity (a.u.)
5
5
5
5
5
5
5
5
*
*
C
D
SOD1
SOD1+D
C
D
SOD1
SOD1+D
Inner
Outer

Figure 4

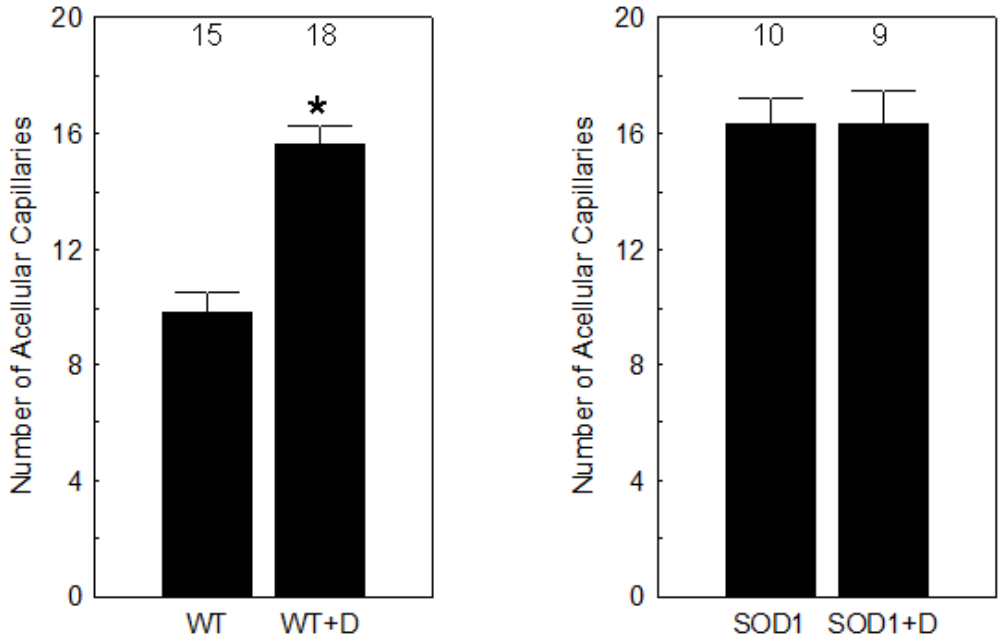
20
16
12
8
4
0
Number of Acellular Capillaries
15
18
*
WT
WT+D
10
9
SOD1
SOD1+D

Reference List

(1) Grunwald JE, Riva CE, Brucker AJ, Sinclair SH, Petrig BL. Altered retinal vascular response to 100% oxygen breathing in diabetes mellitus. Ophthalmology 1984 December;91(12):1447-52.

(2) Sinclair SH, Grunwald JE, Riva CE, Braunstein SN, Nichols CW, Schwartz SS. Retinal vascular autoregulation in diabetes mellitus. Ophthalmology 1982 July;89(7):748-50.

(3) Trick GL, Berkowitz BA. Retinal oxygenation response and retinopathy. Prog Retin Eye Res 2005 March;24(2):259-74.

(4) Phipps JA, Fletcher EL, Vingrys AJ. Paired-flash identification of rod and cone dysfunction in the diabetic rat. Invest Ophthalmol Vis Sci 2004 December;45(12):4592-600.

(5) Han Y, Bearse MA, Jr., Schneck ME, Barez S, Jacobsen CH, Adams AJ. Multifocal electroretinogram delays predict sites of subsequent diabetic retinopathy. Invest Ophthalmol Vis Sci 2004 March;45(3):948-54.

(6) Barber AJ, Lieth E, Khin SA, Antonetti DA, Buchanan AG, Gardner TW. Neural apoptosis in the retina during experimental and human diabetes. Early onset and effect of insulin. J Clin Invest 1998 August 15;102(4):783-91.

(7) Schaefer S, Kajimura M, Tsuyama S, Uchida K, Sato E, Inoue M et al. Aberrant utilization of nitric oxide and regulation of soluble guanylate cyclase in rat diabetic retinopathy. Antioxid Redox Signal 2003 August;5(4):457-65.

(8) Barber AJ, Antonetti DA, Kern TS, Reiter CE, Soans RS, Krady JK et al. The Ins2Akita mouse as a model of early retinal complications in diabetes. Invest Ophthalmol Vis Sci 2005 June;46(6):2210-8.

(9) Barber AJ. A new view of diabetic retinopathy: a neurodegenerative disease of the eye. Prog Neuropsychopharmacol Biol Psychiatry 2003 April;27(2):283-90.

(10) Budzynski E, Wangsa-Wirawan N, Padnick-Silver L, Hatchell D, Linsenmeier R. Intraretinal pH in diabetic cats. Curr Eye Res 2005 March;30(3):229-40.

(11) Ottlecz A, Bensaoula T, Eichberg J, Peterson RG. Angiotensin-converting enzyme activity in retinas of streptozotocin-induced and Zucker diabetic rats. The effect of angiotensin II on Na+,K(+)-ATPase activity. Invest Ophthalmol Vis Sci 1996 October;37(11):2157-64.

(12) Kern TS, Kowluru RA, Engerman RL. Abnormalities of retinal metabolism in diabetes or galactosemia: ATPases and glutathione. Invest Ophthalmol Vis Sci 1994 June;35(7):2962-7.

(13) Ottlecz A, Garcia CA, Eichberg J, Fox DA. Alterations in retinal Na+, K(+)-ATPase in diabetes: streptozotocin-induced and Zucker diabetic fatty rats. Curr Eye Res 1993 December;12(12):1111-21.

(14) MacGregor LC, Matschinsky FM. Altered retinal metabolism in diabetes. II. Measurement of sodium-potassium ATPase and total sodium and potassium in individual retinal layers. J Biol Chem 1986 March 25;261(9):4052-8.

(15) Zhang P, Hatter A, Liu B. Manganese chloride stimulates rat microglia to release hydrogen peroxide. Toxicol Lett 2007 September 10;173(2):88-100.

(16) Di Leo MA, Santini SA, Cercone S, Lepore D, Gentiloni SN, Caputo S et al. Chronic taurine supplementation ameliorates oxidative stress and Na+ K+ ATPase impairment in the retina of diabetic rats. Amino Acids 2002;23(4):401-6.

(17) Berkowitz BA, Roberts R, Stemmler A, Luan H, Gradianu M. Impaired apparent ion demand in experimental diabetic retinopathy: correction by lipoic Acid. Invest Ophthalmol Vis Sci 2007 October;48(10):4753-8.

(18) Ottlecz A, Bensaoula T. Captopril ameliorates the decreased Na+,K(+)-ATPase activity in the retina of streptozotocin-induced diabetic rats. Investigative Ophthalmology Visual Science 1996 July 1;37(8):1633-41.

(19) Zhang JZ, Xi X, Gao L, Kern TS. Captopril Inhibits Capillary Degeneration in the Early Stages of Diabetic Retinopathy. Current Eye Research 2007;32(10):883-9.

(20) Ottlecz A, Bensaoula T. Captopril ameliorates the decreased Na+,K(+)-ATPase activity in the retina of streptozotocin-induced diabetic rats. Investigative Ophthalmology Visual Science 1996 July 1;37(8):1633-41.

(21) Kowluru RA, Atasi L, Ho YS. Role of mitochondrial superoxide dismutase in the development of diabetic retinopathy. Invest Ophthalmol Vis Sci 2006 April;47(4):1594-9.

(22) Sadi G, Yilmaz O, Guray T. Effect of vitamin C and lipoic acid on streptozotocin-induced diabetes gene expression: mRNA and protein expressions of Cu-Zn SOD and catalase. Mol Cell Biochem 2008 February;309(1-2):109-16.

(23) Kanwar M, Chan PS, Kern TS, Kowluru RA. Oxidative Damage in the Retinal Mitochondria of Diabetic Mice: Possible Protection by Superoxide Dismutase. Investigative Ophthalmology Visual Science 2007 August 1;48(8):3805-11.

(24) Kowluru RA, Kowluru V, Xiong Y, Ho YS. Overexpression of mitochondrial superoxide dismutase in mice protects the retina from diabetes-induced oxidative stress. Free Radic Biol Med 2006 October 15;41(8):1191-6.

(25) Marklund SL. Extracellular superoxide dismutase and other superoxide dismutase isoenzymes in tissues from nine mammalian species. Biochem J 1984 September 15;222(3):649-55.

(26) Behndig A, Svensson B, Marklund SL, Karlsson K. Superoxide dismutase isoenzymes in the human eye. Invest Ophthalmol Vis Sci 1998 March;39(3):471-5.

(27) Okado-Matsumoto A, Fridovich I. Subcellular Distribution of Superoxide Dismutases (SOD) in Rat Liver. Cu,Zn-SOD IN MITOCHONDRIA. Journal of Biological Chemistry 2001 October 12;276(42):38388-93.

(28) Levkovitch-Verbin H, Harris-Cerruti C, Groner Y, Wheeler LA, Schwartz M, Yoles E. RGC death in mice after optic nerve crush injury: oxidative stress and neuroprotection. Invest Ophthalmol Vis Sci 2000 December;41(13):4169-74.

(29) Klaeger C, de Sa L, Klaeger AJ, Carlson EJ, Good WV, Epstein CJ. An elevated level of copper zinc superoxide dismutase fails to prevent oxygen induced retinopathy in mice. Br J Ophthalmol 1996 May;80(5):429-34.

(30) Dong A, Shen J, Krause M, Akiyama H, Hackett SF, Lai H et al. Superoxide dismutase 1 protects retinal cells from oxidative damage. J Cell Physiol 2006 September;208(3):516-26.

(31) Kowluru RA, Kern TS, Engerman RL. Abnormalities of retinal metabolism in diabetes or experimental galactosemia. IV. Antioxidant defense system. Free Radic Biol Med 1997;22(4):587-92.

(32) Kowluru RA, Kern TS, Engerman RL, Armstrong D. Abnormalities of retinal metabolism in diabetes or experimental galactosemia. III. Effects of antioxidants. Diabetes 1996 September;45(9):1233-7.

(33) Kowluru R. Retinal metabolic abnormalities in diabetic mouse: Comparison with diabetic rat. Curr Eye Res 2002 February;24(2):123-8.

(34) Lin YJ, Koretsky AP. Manganese ion enhances T1-weighted MRI during brain activation: an approach to direct imaging of brain function. Magn Reson Med 1997 September;38(3):378-88.

(35) Yu X, Wadghiri YZ, Sanes DH, Turnbull DH. In vivo auditory brain mapping in mice with Mn-enhanced MRI. Nat Neurosci 2005 July;8(7):961-8.

(36) Berkowitz BA, Roberts R, Luan H, Bissig D, Bui BV, Gradianu M et al. Manganese-enhanced MRI studies of alterations of intraretinal ion demand in models of ocular injury. Invest Ophthalmol Vis Sci 2007 August;48(8):3796-804.

(37) Berkowitz BA, Roberts R, Penn JS, Gradianu M. High-resolution manganese-enhanced MRI of experimental retinopathy of prematurity. Invest Ophthalmol Vis Sci 2007 October;48(10):4733-40.

(38) Braun RD, Gradianu M, Vistisen KS, Roberts RL, Berkowitz BA. Manganese-enhanced MRI of human choroidal melanoma xenografts. Invest Ophthalmol Vis Sci 2007 March;48(3):963-7.

(39) Wendland MF. Applications of manganese-enhanced magnetic resonance imaging (MEMRI) to imaging of the heart. NMR Biomed 2004 December;17(8):581-94.

(40) Berkowitz BA, Roberts R, Goebel DJ, Luan H. Noninvasive and Simultaneous Imaging of Layer-Specific Retinal Functional Adaptation by Manganese-Enhanced MRI. Investigative Ophthalmology Visual Science 2006 June 1;47(6):2668-74.

(41) Lu H, Xi ZX, Gitajn L, Rea W, Yang Y, Stein EA. Cocaine-induced brain activation detected by dynamic manganese-enhanced magnetic resonance imaging (MEMRI). Proc Natl Acad Sci U S A 2007 February 13;104(7):2489-94.

(42) Craven PA, Melhem MF, Phillips SL, DeRubertis FR. Overexpression of Cu2+/Zn2+ superoxide dismutase protects against early diabetic glomerular injury in transgenic mice. Diabetes 2001 September;50(9):2114-25.

(43) Epstein CJ, Avraham KB, Lovett M, Smith S, Elroy-Stein O, Rotman G et al. Transgenic mice with increased Cu/Zn-superoxide dismutase activity: animal model of dosage effects in Down syndrome. Proc Natl Acad Sci U S A 1987 November;84(22):8044-8.

(44) Schupp DG, Merkle H, Ellermann JM, Ke Y, Garwood M. Localized detection of glioma glycolysis using edited 1H MRS. Magn Reson Med 1993 July;30(1):18-27.

(45) Kern TS, Engerman RL. Pharmacological inhibition of diabetic retinopathy: aminoguanidine and aspirin. Diabetes 2001 July;50(7):1636-42.

(46) Zheng L, Szabo C, Kern TS. Poly(ADP-Ribose) Polymerase Is Involved in the Development of Diabetic Retinopathy via Regulation of Nuclear Factor-{kappa}B. Diabetes 2004 November 1;53(11):2960-7.

(47) Berkowitz BA. Adult and newborn rat inner retinal oxygenation during carbogen and 100% oxygen breathing. Comparison using magnetic resonance imaging delta Po2 mapping. Invest Ophthalmol Vis Sci 1996 September;37(10):2089-98.

(48) Cheng H, Nair G, Walker TA, Kim MK, Pardue MT, Thule PM et al. Structural and functional MRI reveals multiple retinal layers. Proc Natl Acad Sci U S A 2006 November 14;103(46):17525-30.

(49) Liang Z. Longitudinal data analysis using generalized linear models. Biometrika 1986 January 1;73:13-22.

(50) Silva AC, Lee JH, Aoki I, Koretsky AP. Manganese-enhanced magnetic resonance imaging (MEMRI): methodological and practical considerations. NMR Biomed 2004 December 23;17(8):532-43.

(51) Martin PM, Roon P, Van Ells TK, Ganapathy V, Smith SB. Death of retinal neurons in streptozotocin-induced diabetic mice. Invest Ophthalmol Vis Sci 2004 September;45(9):3330-6.

(52) Zhou X, Xie J, Shen M, Wang J, Jiang L, Qu J et al. Biometric measurement of the mouse eye using optical coherence tomography with focal plane advancement. Vision Research 2008 April;48(9):1137-43.

(53) Remtulla S, Hallett PE. A schematic eye for the mouse, and comparisons with the rat. Vision Res 1985;25(1):21-31.

(54) Berkowitz BA, Gradianu M, Schafer S, Jin Y, Porchia A, Iezzi R et al. Ionic Dysregulatory Phenotyping of Pathologic Retinal Thinning with Manganese-enhanced MRI. Investigative Ophthalmology Visual Science 2008 March 24;iovs.

(55) Cooper GJS, Chan YK, Dissanayake AM, Leahy FE, Keogh GF, Frampton CM et al. Demonstration of a Hyperglycemia-Driven Pathogenic Abnormality of Copper Homeostasis in Diabetes and Its Reversibility by Selective Chelation: Quantitative Comparisons Between the Biology of Copper and Eight Other Nutritionally Essential Elements in Normal and Diabetic Individuals. Diabetes 2005 May 1;54(5):1468-76.

(56) Walter RM, Jr., Uriu-Hare JY, Olin KL, Oster MH, Anawalt BD, Critchfield JW et al. Copper, zinc, manganese, and magnesium status and complications of diabetes mellitus. Diabetes Care 1991 November;14(11):1050-6.

(57) Failla ML, Kiser RA. Altered tissue content and cytosol distribution of trace metals in experimental diabetes. J Nutr 1981 November;111(11):1900-9.

(58) Berkowitz BA, Gradianu M, Schafer S, Jin Y, Porchia A, Iezzi R et al. Ionic Dysregulatory Phenotyping of Pathologic Retinal Thinning with Manganese-enhanced MRI. Investigative Ophthalmology Visual Science 2008 March 24;iovs.

(59) Osborne NN, Casson RJ, Wood JP, Chidlow G, Graham M, Melena J. Retinal ischemia: mechanisms of damage and potential therapeutic strategies. Prog Retin Eye Res 2004 January;23(1):91-147.

(60) Kowluru RA, Kanwar M, Kennedy A. Metabolic memory phenomenon and accumulation of peroxynitrite in retinal capillaries. Exp Diabetes Res 2007;2007:21976.

(61) Kern TS, Engerman RL. A mouse model of diabetic retinopathy. Arch Ophthalmol 1996 August;114(8):986-90.

(62) DeRubertis FR, Craven PA, Melhem MF, Salah EM. Attenuation of Renal Injury in db/db Mice Overexpressing Superoxide Dismutase: Evidence for Reduced Superoxide-Nitric Oxide Interaction. Diabetes 2004 March;53(3):762-8.

(63) Craven PA, Melhem MF, Phillips SL, DeRubertis FR. Overexpression of Cu2+/Zn2+ superoxide dismutase protects against early diabetic glomerular injury in transgenic mice. Diabetes 2001 September;50(9):2114-25.

(64) Berkowitz BA, Gradianu M, Schafer S, Jin Y, Porchia A, Iezzi R et al. Ionic Dysregulatory Phenotyping of Pathologic Retinal Thinning with Manganese-enhanced MRI. Investigative Ophthalmology Visual Science 2008 March 24;iovs.